Rendering of Human Teeth and Restorative Biomaterials

Jin Woo Jung(1), Gary Meyer(1), Ralph DeLong(2), and Brian N. Holmes(3)
(1) Computer Science and Engineering Department, University of Minnesota; Minneapolis, MN USA
(2) Minnesota Dental Research Center for Biomaterials and Biomechanics, University of Minnesota; Minneapolis, MN USA
(2) 3M ESPE Dental Products Laboratory; St. Paul, MN USA

Abstract

A tooth is a heterogeneously structured object of translucent materials, such as enamel and dentin. The correct simulation of the appearance of teeth is useful in the field of dental restoration to detect the correct color and to develop materials for restoration. However, conventional surface reflection models do not capture the appearance of translucent materials accurately, because they assume that the rays of light are just reflected off the surface. For translucent objects, light not only bounces off the surface, but also interacts with the material under the surface. Therefore, physically correct rendering of teeth must take this into account to understand and model subsurface scattering. This paper discusses the optical characteristics of enamel and dentin. In addition, rendered images using volume photon mapping with Monte Carlo photon tracing are presented for enamel, dentin and biomaterials.

1. Introduction

Realistic visualization has long been one of the most important objectives in computer graphics. However, many light effects are too complex to produce convincing rendered images using existing computer graphic techniques. In particular, realistic image synthesis for translucent materials has been a perennial challenge of computer graphics, even though the materials, such as paper, skin, marble, jade, fog, clouds, dusty air, smoke, fire, and silty water, are very common in everyday life. Unlike metal and matte, the modeling of these participating media with simple bidirectional reflectance distribution functions (BRDFs) does not provide convincing images. In translucent materials, light is not only reflected off the surface of an object, but it also penetrates the surface, is scattered within the object, and leaves the object in various directions. The object must appear smooth and soft, blurring surface geometric details. This light transport mechanism is commonly known as subsurface scattering. The modeling of subsurface scattering is able to dramatically increase the realism of the translucent materials in computer graphics images.

Because an understanding of light propagation in biological tissues is essential for effective applications of light in medical diagnostics and therapeutics, computer graphics can make significant contributions in this field through the simulation of light transport in the tissues [1-3]. Especially in the field of dentistry, computer graphics can play an important role to break through many challenges. Appropriate computer images can help people understand the anatomy of teeth and their appearance, and knowledge about light propagation through tissues can aid in successful treatments, such as probing for the detection of dental caries [3]. In addition, computer graphics has been widely used to handle three dimensional objects on a computer screen for research or treatment. Especially, the physically correct rendering of teeth is expected to be important in the field of dental restoration. In this field, the aesthetics of teeth, as well as their functions, are important goals. So far, the color of dental restorative materials has either been ignored or estimated visually with shade guides. Therefore, the physically correct appearance on the computer screen can help people understand the optical characteristics of biomaterials and know which restoration materials are appropriate for fillers or crowns.

In this paper, physically correct rendering methods to capture the appearance of teeth are discussed and rendered images are presented to show the usability of these approaches. The rest of this paper is organized as follows. Section 2 discusses related work for subsurface light transport and analytic models for these phenomena. Section 3 introduces the physical characteristics of human teeth for enamel and dentin. Section 4 discusses the Monte Carlo photon tracing method for full simulation of subsurface scattering based on volume photon mapping. Section 5 presents the simulation results of photon tracing and the rendered images for teeth and some materials that have known optical characteristics. Finally, section 6 concludes the paper and discusses future work.

2. Related work

Because of its computational complexity, subsurface scattering has been traditionally ignored or simply approximated using Lambertian diffuse reflection. However, the BRDF that is considered in this approximation accounts for scattering only at a single point, and it cannot be used to simulate light transport within the material between different points on the surface. More accurate models have been done through photon mapping, path tracing, and the scattering equation with high performance computers and dedicated graphic devices. Dorsey et al. [4] treated the material as a participating medium and used volume photon mapping, Jensen et. al [5] used path tracing and Pharr et al. [6] used scattering equations. These approaches are more complete than before and produce convincing translucent objects on the computer screen, but rendering done using these approaches is still computationally costly. In order to model these translucent materials for efficient rendering, diffusion approximation has been widely employed. Because the materials are assumed to be optically dense, multiple scattering can be approximated by a diffusion process described by the diffusion equation. Jensen et al. [7] formulated a bidirectional surface scattering reflectance distribution function (BSSRDF) for homogeneous materials with dipole diffusion approximation and Wang et al. [8] introduced an efficient way to solve the diffusion equation for heterogeneous materials using a finite difference method (FDM).

Jensen et al. [7] presented the BSSRDF as the sum of single scattering and a diffuse dipole approximation for multiple scattering in homogeneous materials. Jensen et al. [8] then presented a two-pass hierarchical integration technique to significantly accelerate the computation of multiple scattering components. In the first pass, the light incident on the surfaces of all translucent objects is calculated. The second pass uses this pre-computed irradiance to calculate the subsurface transport at each shading point for all pixels. Dipole diffusion approximation assumes that the medium is modeled as having an isotropic phase function with appropriately modified scattering and extinction coefficient for any anisotropic scattering medium with a high albedo [9]. Therefore, it does not account for any anisotropic characteristic of the materials.

Donner et al. [10, 11] introduced extensions to the dipole diffusion approximation that allow correct rendering of thin slabs of material and right angle edges. While the dipole diffusion approximation assumes that the material is homogeneous and semi-infinitely thick, multi-pole diffusion approximation is able to do the correct rendering of thin slabs, such as a piece of paper, or even multilayered heterogeneous materials like skin by convolving the diffusion profiles of multiple layers. In addition, to render the material that is non-flat and finite in extent, Donner et al. [11] introduced a quad-pole diffusion approximation model for right angle edges and showed that the appropriate linear combination of dipole diffusion reflectance, multi-pole diffusion reflectance, and quad-pole diffusion reflectance are able to do physically correct rendering for an object that has complex geometry, with photon diffusion.

While the analytic solution with dipole, multi-pole and quad-pole diffusion approximations render homogeneous materials well, they require solving a diffusion equation whose boundary condition is defined by the given illumination conditions for heterogeneous materials, because every point in the volume has a different diffusion coefficient and absorption coefficient. Wang et al. [12] introduced the polygrid diffusion algorithm by constructing a polygrid in a 3D model to solve the diffusion equation using an FDM. This algorithm represents an object as a polygrid that has regular connectivity and an irregular shape. The regular connectivity makes it available for this algorithm to be implemented on a GPU for real-time performance. However, this method is restricted to objects with simple geometry (low genus, no sharp features), because it uses cubic grids. Instead of cubic grids, Wang et al. [13] discretize translucent objects using tetrahedral grids to handle arbitrary geometry.

The problem of photon propagation in participating media can be treated as a random-walk process, so it can be modeled accurately using Monte Carlo simulation [14]. However, Monte Carlo simulation takes a long time to obtain results because comprehensive simulation for every combination of absorption and scattering coefficients is required to find optimal optical parameters. On the other hand, for important idealized situations, an analytic solution for light transport in translucent objects is able to provide these parameters in a short time.

For homogenous media, the telegrapher's equation, the diffusion equation, and multiple-flux theories such as the Kubelka-Munk and four-flux theories are available as an analytic model of the subsurface light transport that takes into account the transmission and reflection density [14]. Since Kubelka and Munk introduced a theory for the analysis of diffuse reflectance spectra from weakly absorbing material, the photon propagation problem in translucent media has been formulated as a random-walk process and simplified to a simple diffusion problem. However, these approaches fail, if a significant amount of absorption is present within the volume [14]. Another analytic model for the random-walk process is the telegrapher's equation, which has been shown to be a significant improvement over the diffusion equation. Kong et al. [14] demonstrate that the solution of the telegrapher's equation comes closest to the Monte Carlo simulation data for optical transmission and reflection density of translucent media.

Since translucent materials have been approximated using a simple BRDF model, many alternative approaches have been considered to improve the quality and speed of rendering. It has been shown that full Monte Carlo simulation based on photon mapping, path tracing, and the scattering equation produces convincing images. However, this approach is computationally expensive. Therefore, diffusion approximation has been considered for faster rendering. In addition, geometrically simple models were introduced to make the problem tractable. In this paper, full Monte Carlo simulations based on volume photon mapping are employed to make a ground truth picture, even though they are computationally expensive.

3. Physical characteristic of human teeth

The primary function of teeth associated with humans is mastication for nutrition. However, they are also essential for appropriate speech and aesthetics [15]. The tooth is composed of two hard tissues, the enamel and the dentin. The enamel is a hard, inert, acellular tissue which is supported by the dentin. The dentin is a less mineralized, more resilient, and vital hard connective tissue, whose formative cells are in and supported by the dental pulp, a soft connective tissue. The enamel and the dentin make

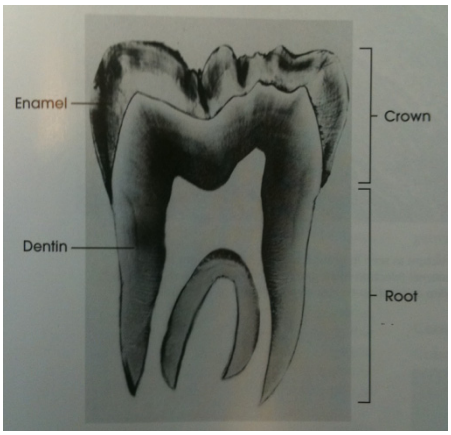

Figure 1 Ground section of a tooth [15]

teeth hard and resilient. In addition, both tissues give teeth a unique permanence, because they are mineralized.

Anatomically the tooth is divided into a crown and a root. The junction between the two parts is called the cervical margin. The term clinical crown denotes that part of the tooth visible in the oral cavity. The majority of the crown is composed of dentin with the pulp chamber inside, while the outer part of the crown is enamel. Therefore, the color of a tooth is decided by the enamel, the dentin and the pulp. Although teeth vary considerably in shape and size, histologically they are similar.

For optical properties, studies have shown that dentin and enamel weakly absorb light and light scattering plays an important role in determining the deposited energy distribution in the tissue [3]. Therefore, light scattering is a key factor in determining the color of teeth. In addition, dental hard tissues are inhomogeneous materials. Dental enamel is an ordered array of inorganic apatite-like crystals, and dentin is a complex structure, honeycombed with dentinal tubules. The complex nature of enamel and dentin makes the scattering distribution anisotropic and dependent on tissue orientation relative to the irradiating light source and its spatial location.

4. Volume photon mapping with Monte Carlo photon tracing

Monte Carlo photon tracing is the first method that fully simulated subsurface scattering based on photon mapping [4, 5, 16]. When a photon enters a participating medium, it can either continue unaffected through the medium or it can interact with the medium at a given location. When a photon interacts with a medium, it is either absorbed or scattered. Using the volume photon map, which contains information of photon's interaction and ray marching, subsurface scattering can be simulated almost completely.

Monte Carlo Photon tracing

While a photon map is required to simulate global illumination for opaque materials, a volume photon map needs to be built to simulate subsurface scattering in translucent materials. When a photon is scattered or absorbed, it is stored into the photon map.

The average distance, d, which a photon moves through a medium before the next interaction is decided by the extinction coefficient $\sigma_t = \sigma_s + \sigma_a$ and given by the following:

$$\mathrm{d} = \frac{1}{\sigma_t} \tag{1}$$

The power of the photon that travels through the medium is reduced by $\mathrm{e}^{-\sigma_t s}$, where s is the distance that the photon moves. Assuming that each power reduction level has the same probability, the distance to the next interaction is decided by the following:

$$\mathrm{d} = -\frac{\ln \xi}{\sigma_t} \tag{2}$$

where $\xi \in]0,1]$ is a uniformly distributed random number. Because the traveling distance varies depending on the extinction coefficient, it is not necessary to scale down the photon powers when they are traveling within the volume.

At the point of interaction the photon is either absorbed or scattered. The probability of scattering is decided by the scattering coefficient, σ_s, and the extinction coefficient, σ_t, and given by the scattering albedo,

$$\Lambda = \frac{\sigma_s}{\sigma_t} \tag{3}$$

In order to determine whether the photon is scattered or absorbed, Russian roulette is used in the following way:

$$\text{Given } \xi \in [0,1] \rightarrow \begin{cases} \xi \leq \Lambda & \text{Photon is scattered} \\ \xi > \Lambda & \textit{Photon is absorbed} \end{cases} \tag{4}$$

If the photon is scattered it will continue without changing power. For photons that carry information for multiple wavelengths, it might be necessary to use an average albedo, and then scale the individual components of the scattered photon, because each color band has a different scattering coefficient. Although this approach generally gives a good approximation for the intensity scale in each color component when the photons interact within the volume, it does not guarantee the correct simulation of the photon's power in each wavelength or color component. On the other hand, it can be simulated for some wavelengths, and then a final image can be reconstructed using interpolation.

The direction of the scattered photon depends on the phase function. The phase function $\mathrm{p}(x, \vec{\omega}', \vec{\omega})$ describes the amount of light scattered to the direction $\vec{\omega}'$ at position x for the light incident from the $\vec{\omega}$ direction. Thus, the phase function is the probability distribution of the scattered light, and it must integrate to one over all angles:

$$\int_{\Omega_{4\pi}} \mathrm{p}(x, \vec{\omega}', \vec{\omega}) d\vec{\omega}' = 1 \tag{5}$$

When the phase function is circularly symmetrical round the axis of the incident beam, it depends only on the angle, θ, between the incoming ray from the $\vec{\omega}$ direction and the scattered ray into the direction $\vec{\omega}'$, and it can be written as $\mathrm{p}(\theta)$.

The average cosine of the scattered direction can specify the preferred scattering direction of the phase function. It is denoted by $\mathrm{g}(x)$ and defined as the integral over the sphere multiplied by the cosine of the angle, θ.

$$g(x) = \int_{\Omega_{4\pi}} \mathrm{p}(x, \vec{\omega}', \vec{\omega})(\vec{\omega}' \cdot \vec{\omega}) d\vec{\omega}' \tag{6}$$

The phase functions for a transparent material are often highly anisotropic so a uniform sampling is very inefficient. Therefore, importance sampling has to be considered with its phase function [17].

The most commonly used phase function is the empirical Henyey-Greenstein phase function, given by the following:

$$\mathrm{p}(\theta) = \frac{1 - g^2}{4\pi(1 + g^2 - 2g\cos\theta)^{1.5}} \tag{7}$$

where $g \in]-1, 1[$ is an *asymmetry parameter* equal to the average cosine of the scattered directions. Positive g gives forward scattering and negative g gives backward scattering. Note that g = 0 is isotropic scattering.

For more complex types of scattering, a combination of several functions can be considered.

$$\mathrm{p}(\theta) = \sum_{i=1}^{N} \omega_i \frac{1 - {g_i}^2}{4\pi(1 + {g_i}^2 - 2g_i\cos\theta)^{1.5}} \tag{8}$$

where $\sum_{i=1}^{N} \omega_i = 1$ and g_i controls the shape of each lobe and ω_i is the weight.

Given the incoming direction of a photon, the angle, θ, of the new scattered direction is given by:

$$\cos\theta = \frac{1}{2g}\left(1 + g^2 - \left(\frac{1 - g^2}{1 - g + 2g\xi}\right)^2\right) \tag{9}$$

where ξ is a uniform random number between zero and one.

In this paper, a linear combination of HG phase functions and an isotropic scattering phase function is used with the anisotropy parameters that were determined by Fried et al. [3]. The linear combination of the functions is given by:

$$\mathrm{p}(\theta) = f_d\frac{1}{4\pi} + (1 - f_d)\left(\frac{1 - {g_i}^2}{4\pi(1 + {g_i}^2 - 2g_i\cos\theta)^{1.5}}\right) \tag{10}$$

The photons coming directly from the light source will be computed using a standard ray-tracing technique, and hence will not be stored in the volume photon map.

Rendering

When a ray enters a translucent material, it is refracted into the medium. Ray marching is used to evaluate the contribution from the medium along the refracted ray. In-scattered radiance is the sum of a direct single-scattering term and an indirect multiple-scattering term. The indirect multiple-scattering term is computed using the volume radiance estimated. Ray marching computes the radiance by recursively calling the formula to move backwards through the medium.

$$\begin{aligned} L_{n+1} = &\sum_{l}^{N} L_l(x, \vec{\omega}'_l)p(x, \vec{\omega}'_l, \vec{\omega})\sigma_s(x)\Delta x \\ &+ \left\{\sum_{p=1}^{n} p\left(x, \vec{\omega}'_p, \vec{\omega}\right)\frac{\Delta\Phi_p\left(x, \vec{\omega}'_p\right)}{\frac{4}{3}\pi r^3}\right\}\Delta x \\ &+ e^{-\sigma_t(x)\Delta x}L_n(x + \Delta x, \vec{\omega}) \end{aligned} \tag{11}$$

where N is the number of light sources in the scene, L_l is the radiance from each light source, n is the number of the nearest photons within the volume of the sphere, $(4/3\pi r^3)$, and $\Delta\Phi_p$ is the flux carried by the photons that correspond to the indirect illumination. The first term accounts for the contribution from the segment due to direct illumination, the second term is the radiance due to multiple scattering, and the last term is the radiance entering the segment at the backside.

Note that direct illumination must be attenuated properly based on the distance that the shadow ray moves through the medium. For non-homogeneous media, this might need to be integrated using another ray-marching evaluation. The power reduction of each light is computed in the following way:

$$L_l(x, \vec{\omega}'_l) = e^{-\sigma_t d}L_e(x, \vec{\omega}'_l) \tag{12}$$

Since ray-tracing is used inside the material, a visibility test using a shadow ray has to consider the refraction of the light. However, the configuration for the refraction is difficult to compute exactly. In order to consider the refraction of the shadow ray, the photon map for all types of illumination is required. However, direct illumination can be estimated more accurately by estimating the true distance that the ray would have moved through the material.

$$d'_i = d_i\frac{|\vec{\omega}\cdot\vec{n}|}{\sqrt{1 - \left(\frac{1}{\eta}\right)^2(1 - |\vec{\omega}\cdot\vec{n}|^2)}} \tag{13}$$

5. Simulation and rendering

Rendering of biomaterials with known optical characteristics

The transmittance and reflectance of a disc made out of a biomaterial were measured for D65 and three wavelengths, 450 nm, 540 nm and 605 nm. Then optical parameters were calculated based on the telegrapher's equation. Table 1 shows the measured data for normally incident light.

	TT	TR	TA	*n*	*g*
D65	61.21%	32.28%	6.51%	1.540	0.75
450 nm	48.97%	30.16%	20.87%	1.550	0.75
540 nm	60.16%	32.43%	7.41%	1.540	0.75
605 nm	65.40%	32.55%	2.05%	1.537	0.75

Table 1 Measured data from the biomaterial

** TT: total transmittance*

** TR: total reflectance*

** TA: total absorption*

** n: refractive index.*

** g: average cosine of the scattering angle relative to the angle of incidence for a single scattering event.*

** Sample thickness = 0.5 mm*

Then Monte Carlo photon tracing was performed based on the information in three wavelengths, 450 nm, 540 nm, and 605 nm. Whenever photons are scattered and absorbed, they are stored in the volume photon map. In this simulation, 100,000,000 photons were collected and used for rendering. Because those photons were collected for three wavelengths, it was necessary to reconstruct a final image by interpolating values between known wavelengths after estimating the photon densities for each spectrum. Figure 2 shows the spectral power distributions for a D65 light source and the interpolated transmitted powers. Since the wavelengths where the transmittance was measured are relatively close, it was assumed that linear interpolation between the known values can predict the values between the known wavelengths. However, it accounts for only 24.15 % of the transmitted power, although 61.21 % of the power is transmitted through the material. In order to address the spectral response outside the known range, extrapolation is necessary.

When determining the basis for interpolation and extrapolation, the transmittance and the reflectance for D65 light can be boundary conditions, because the total transmittance and reflectance of the material for D65 light were measured. However, there is no analytic solution to determine the basis, because infinite combinations of the basis can satisfy the boundary conditions. Because the unknown values exist in a low and high spectrum, different basis affect red and blue colors. More weight on the lower spectrum range will add more blue or magenta color, while more weight on the higher spectrum range will add more red color.

Figure 3 shows the rendered image of 5 mm thick discs. In this figure, the disc on the left side is right on the check pattern ribbon and the disc on the right side is 5 mm away from the ribbon. The disc on the left side shows a clear checker pattern of the ribbon, while the disc away from the ribbon shows no distinct pattern. When the disc is right on the ribbon, the light transmitted through the object is bounced off the ribbon and into the volume again. In addition, the reflected photons are localized, because there is no room for photons to travel far between the disc and the ribbon. The

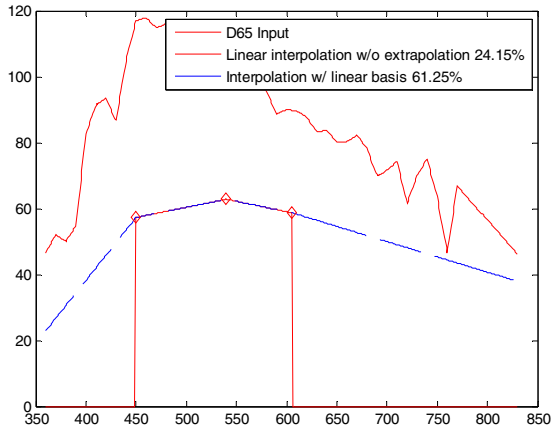

Figure 2 Spectral power distribution for D65 and the interpolated transmitted powers

disc is not thick enough to scatter photons and obscure the pattern on the surface either. On the other hand, the light transmitted through the disc on the right side is scattered into various directions and reflected off the ribbon. Furthermore, the reflected light enters a wider area of the volume, so it opacifies the pattern on the surface.

In Figure 4, an identical simulation has been performed using enamel instead of the biomaterial. Unlike yellowish color of the biomaterial, light blue-gray is observed in this figure. This rendering result agrees the fact that the enamel of a natural tooth is opalescent [18]. To facilitate the comparison of scattering effects, the optical thickness of the enamel was adjusted to have the same transparency as the biomaterial. Notice that the visibility of the checkerboard beneath the two enamel discs is similar to the visibility of the checkerboard underneath the two discs made from the biomaterial. This demonstrates that the biomaterial has translucent properties that are comparable to those of the enamel.

Rendering of teeth using volume photon mapping

In order to render a tooth, appropriate optical parameters were chosen**.** The scattering and absorption coefficients follow the wavelength dependency that was determined by Spitzer et al. and Bosch et al. [19, 20]. Refractive indices and anisotropy parameters are from the data Fried et al. introduced [3]. Because Bosch et al. showed that dentin is highly anisotropic and its optical characteristic varies depending on its position, the scattering and absorption coefficients are scaled proportionately [20]. Pulp was not considered in this rendering, because the optical thickness of the dentin is high enough to ignore the contribution of the pulp [20]. In addition, anisotropy parameters were scaled to permit rendering with a limited number of photons. When the anisotropy parameters are too large, the photons become locally concentrated requiring a larger number of photons to render a wide area. In this simulation, 100,000,000 photons were used to render the teeth and 1,000,000 photons were captured for global illumination. Figure 5 is the image in which three teeth were in the Cornell box.

The preliminary results in Figures 3, 4, and 5 demonstrate our current ability to independently simulate the enamel of a real tooth, the biomaterial for use in restorations, and the anatomy of a physical tooth. We are working on the simulation of a crown composed of biomaterial that will be attached to the base of a three-dimensional tooth. This will permit comparisons between simulated real teeth and simulated restorations.

6. Discussion and conclusion

In the visible range, dentin and enamel absorb light weakly, and light scattering plays an essential role in determining the appearance of teeth. Especially, when compared to dentin, enamel absorption is negligible. Because of the complicated structure of these materials, the scattering distributions are generally anisotropic and depend on the orientation of crystallites and tubules.

Volume photon mapping captures the photons that are entering into teeth and computes the density of the photons to calculate the color on the surface. In this way, the appearance of teeth can be

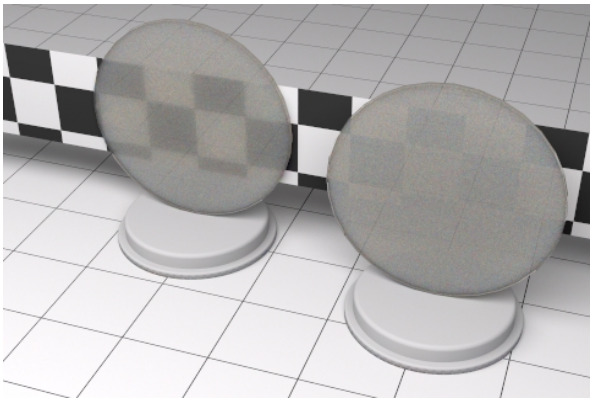

Figure 3 Discs made out of biomaterial on a checker pattern ribbon. The disc on the left side is right on the ribbon, while the disc on the right side is away from the ribbon by 5 mm.

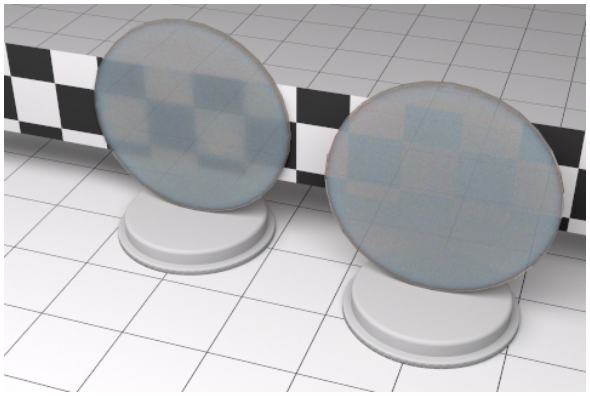

Figure 4 Discs made out of enamel on a checker pattern ribbon. The disc on the left side is right on the ribbon, while the disc on the right side is away from the ribbon by 5 mm.

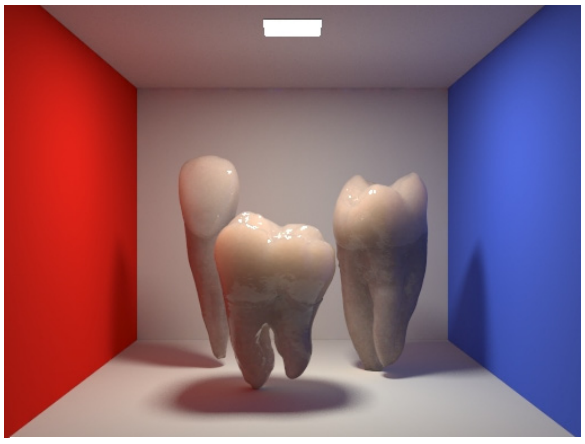

Figure 5 Three teeth in the Cornell box

rendered correctly, but at a high computational cost. It is shown that biomaterials with measured data can be rendered with the volume photon mapping by determining the optical parameters with the analytic solutions.

The rendered images of biomaterials with the known optical characteristics were similar to its real appearance; however, it was difficult to determine how similar to the real sample it was. Small differences in optical parameters and lighting conditions could affect the overall appearance. In addition, the method of interpolation and extrapolation could affect the appearance, because of the limited number of wavelengths that provided spectral responses. Furthermore, Monte Carlo photon tracing of volume photon mapping approximated the scattering process with average scattering albedo and the average cosine of the scattered direction, so it could affect the appearance.

Although it is shown that volume photon mapping simulates the subsurface scattering of teeth, the simulation has limits. First, it is assumed that each material is homogenous. In fact, enamel and dentin have complicated structures and their densities differ at each position. Even more, light scattering depends on the orientation of crystallites and tubules that comprise enamel and dentin. However, those structures were not considered here. Second, the simulations were performed with limited photons. Highly scattered and highly anisotropic material need a large number of photons and requires considerable memory. For this reason, each coefficient and anisotropy parameter was scaled in this simulation.

In the future, it will be necessary to simulate for each wavelength and integrate the spectral responses so that the accurate appearance can be reconstructed on a computer screen. Although analyzing the full spectral responses is computationally expensive, this approach will give us not only accurate rendition of a material, but also the information on the basis functions to reconstruct the full spectral responses of wavelengths.

References

[1] A. Kienle, F. K. Forster, R. Diebolder, and R. Hibst, "Light propagation in dentin: influence of microstructure on anisotropy," *Physics in medicine and biology,* vol. 48, pp. N7-14, Jan 21 2003.

[2] A. Kienle, R. Michels, and R. Hibst, "Magnification--a new look at a long-known optical property of dentin," *Journal of dental research,* vol. 85, pp. 955-9, Oct 2006.

[3] D. Fried, R. E. Glena, J. D. Featherstone, and W. Seka, "Nature of light scattering in dental enamel and dentin at visible and near-infrared wavelengths," *Appl Opt,* vol. 34, pp. 1278-85, Mar 1 1995.

[4] J. Dorsey, A. Edelman, H. W. Jensen, J. Legakis, H. K\, \#248, and h. Pedersen, "Modeling and rendering of weathered stone," presented at the Proceedings of the 26th annual conference on Computer graphics and interactive techniques, 1999.

[5] H. W. Jensen, J. Legakis, J. Dorsey, J. Justin, and L. J. Dorsey, "Rendering of Wet Materials," presented at the Rendering Techniques '99, 1999.

[6] M. Pharr and P. Hanrahan, "Monte Carlo evaluation of non-linear scattering equations for subsurface reflection," presented at the Proceedings of the 27th annual conference on Computer graphics and interactive techniques, 2000.

[7] H. W. Jensen, S. R. Marschner, M. Levoy, and P. Hanrahan, "A practical model for subsurface light transport," presented at the Proceedings of the 28th annual conference on Computer graphics and interactive techniques, 2001.

[8] H. W. Jensen and J. Buhler, "A rapid hierarchical rendering technique for translucent materials," *ACM Trans. Graph.,* vol. 21, pp. 576-581, 2002.

[9] M. Pharr and G. Humphreys, *Physically Based Rendering: From Theory to Implementation*: Morgan Kaufmann Publishers Inc., 2010.
[10] C. Donner and H. W. Jensen, "Light diffusion in multi-layered translucent materials," *ACM Trans. Graph.,* vol. 24, pp. 1032-1039, 2005.
[11] C. Donner and H. W. Jensen, "Rendering translucent materials using photon diffusion," presented at the ACM SIGGRAPH 2008 classes, Los Angeles, California, 2008.
[12] J. Wang, S. Zhao, X. Tong, S. Lin, Z. Lin, Y. Dong, B. Guo, and H.-Y. Shum, "Modeling and rendering of heterogeneous translucent materials using the diffusion equation," *ACM Trans. Graph.,* vol. 27, pp. 1-18, 2008.
[13] Y. Wang, J. Wang, N. Holzschuch, K. Subr, J.-H. Yong, and B. Guo, "Real-time Rendering of Heterogeneous Translucent Objects with Arbitrary Shapes," *Computer Graphics Forum,* vol. 29, pp. 497-506, 2010.
[14] S. H. Kong and J. D. Shore, "Evaluation of the telegrapher's equation and multiple-flux theories for calculating the transmittance and reflectance of a diffuse absorbing slab," *JOSA A,* vol. 24, pp. 702-710, 2007.
[15] R. T. Cate, *Oral Histology: Development, Structure and Function*: Mosby, 1998.
[16] H. W. Jensen and P. H. Christensen, "Efficient simulation of light transport in scences with participating media using photon maps," presented at the Proceedings of the 25th annual conference on Computer graphics and interactive techniques, 1998.
[17] H. W. Jensen, *Realistic image synthesis using photon mapping*: A. K. Peters, Ltd., 2001.
[18] Y. K. Lee, H. Lu, and J. M. Powers, "Measurement of opalescence of resin composites," *Dental materials : official publication of the Academy of Dental Materials,* vol. 21, pp. 1068-74, Nov 2005.
[19] D. Spitzer and J. T. Bosch, "The absorption and scattering of light in bovine and human dental enamel," *Calcified tissue research,* vol. 17, pp. 129-37, 1975.
[20] J. J. t. Bosch and J. R. Zijp, "Optical properties of dentin," in *Dentine and Dentine Reactions in the Oral Cavity*, A. Thylstrup, S. A. Leach, and V. Qvist, Eds., ed: Oxford University Press, 1987.

Author Biography

Jin Woo Jung received his BE in Electrical Engineering and ME in Digital Signal Processing from the Chung-Ang University (Korea). He is currently a PhD student in the Department of Computer Science at the University of Minnesota.